Title

X-ray Crystallographic Structures of a Trimer, Dodecamer, and Annular Pore Formed by an Aβ17-36 β-Hairpin.

Journal

Journal of the American Chemical Society, 138(13)

Authors

Kreutzer, Adam

Hamza, Imane

Spencer, Ryan

et al.

Publication Date

2016-04-06

DOI

10.1021/jacs.6b01332

Peer reviewed

JACS
JOURNAL OF THE AMERICAN CHEMICAL SOCIETY

Article

pubs.acs.org/JACS

X-ray Crystallographic Structures of a Trimer, Dodecamer, and Annular Pore Formed by an Aβ_{17-36} β-Hairpin

Adam G. Kreutzer, Imane L. Hamza, Ryan K. Spencer, and James S. Nowick*

Department of Chemistry, University of California, Irvine, Irvine, California 92697-2025, United States

Supporting Information

ABSTRACT: High-resolution structures of oligomers formed by the β-amyloid peptide Aβ are needed to understand the molecular basis of Alzheimer's disease and develop therapies. This paper presents the X-ray crystallographic structures of oligomers formed by a 20-residue peptide segment derived from Aβ. The development of a peptide in which Aβ_{17-36} is stabilized as a β-hairpin is described, and the X-ray crystallographic structures of oligomers it forms are reported. Two covalent constraints act in tandem to stabilize the Aβ_{17-36} peptide in a hairpin conformation: a δ-linked ornithine turn connecting positions 17 and 36 to create a macrocycle and an intramolecular disulfide linkage between positions 24 and 29. An *N*-methyl group at position 33 blocks uncontrolled aggregation. The peptide readily crystallizes as a folded β-hairpin, which assembles hierarchically in the crystal lattice. Three β-hairpin monomers assemble to form a triangular trimer, four trimers assemble in a tetrahedral arrangement to form a dodecamer, and five dodecamers pack together to form an annular pore. This hierarchical assembly provides a model, in which full-length Aβ transitions from an unfolded monomer to a folded β-hairpin, which assembles to form oligomers that further pack to form an annular pore. This model may provide a better understanding of the molecular basis of Alzheimer's disease at atomic resolution.

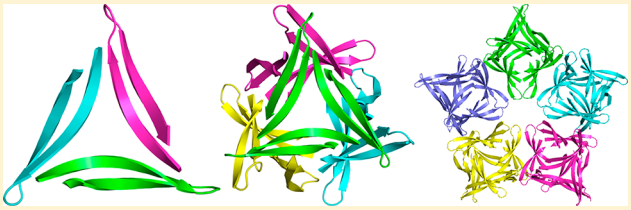

INTRODUCTION

High-resolution structures of oligomers formed by the β-amyloid peptide Aβ are desperately needed to understand the molecular basis of Alzheimer's disease and ultimately develop preventions or treatments. In Alzheimer's disease, monomeric Aβ aggregates to form soluble low molecular weight oligomers, such as dimers, trimers, tetramers, hexamers, nonamers, and dodecamers, as well as high molecular weight aggregates, such as annular protofibrils.[1] Over the last two decades the role of Aβ oligomers in the pathophysiology of Alzheimer's disease has begun to unfold.

Mouse models for Alzheimer's disease have helped shape our current understanding about the Aβ oligomerization that precedes neurodegeneration. Aβ isolated from the brains of young plaque-free Tg2576 mice forms a mixture of low molecular weight oligomers.[2] A 56 kDa soluble oligomer identified by SDS-PAGE was found to be especially important within this mixture. This oligomer was termed Aβ*56 and appears to be a dodecamer of Aβ. Purified Aβ*56 injected intercranially into healthy rats was found to impair memory, providing evidence that this Aβ oligomer may cause memory loss in Alzheimer's disease. Smaller oligomers with molecular weights consistent with trimers, hexamers, and nonamers were also identified within the mixture of low molecular weight oligomers. Treatment of the mixture of low molecular weight oligomers with hexafluoroisopropanol resulted in the dissociation of the putative dodecamers, nonamers, and hexamers into trimers and monomers, suggesting that trimers may be the building block of the dodecamers, nonamers, and hexamers. Recently, Aβ trimers and Aβ*56 were identified in the brains of cognitively normal humans and were found to increase with age.[3]

A type of large oligomers called annular protofibrils (APFs) have also been observed in the brains of transgenic mice and isolated from the brains of Alzheimer's patients. APFs were first discovered *in vitro* using chemically synthesized Aβ that aggregated into porelike structures that could be observed by atomic force microscopy (AFM) and transmission electron microscopy (TEM).[4,5] The sizes of APFs prepared *in vitro* vary among different studies. Lashuel et al. observed APFs with an outer diameter that ranged from 7−10 nm and an inner diameter that ranged from 1.5−2 nm, consistent with molecular weights of 150−250 kDa.[6] Quist et al. observed APFs with an outer diameter of 16 nm embedded in a lipid bilayer.[7] Kayed et al. observed APFs with an outer diameter that ranged from 8−25 nm, which were composed of small spherical Aβ oligomers, 3−5 nm in diameter.[8] Although the APFs in these studies differ in size, they share a similar annular morphology and appear to be composed of smaller oligomers.

APFs have also been observed in the brains of APP23 transgenic mice by immunofluorescence with an anti-APF antibody and were found to accumulate in neuronal processes and synapses.[9] In a subsequent study, APFs were isolated from the brains of Alzheimer's patients by immunoprecipitation with an anti-APF antibody. These APFs had an outer diameter that

Received: February 4, 2016
Published: March 11, 2016

DOI: 10.1021/jacs.6b01332
J. Am. Chem. Soc. 2016, 138, 4634−4642

ranged from 11−14 nm and an inner diameter that ranged from 2.5−4 nm.[10]

Dimers of Aβ have also been isolated from the brains of Alzheimer's patients.[11−13] Aβ dimers inhibit long-term potentiation in mice and promote hyperphosphorylation of the microtubule-associated protein tau, leading to neuritic damage.[14,15] Aβ dimers have only been isolated from human or transgenic mouse brains that contain the pathognomonic fibrillar Aβ plaques associated with Alzheimer's disease. Furthermore, the endogenous rise of Aβ dimers in the brains of Tg2576 and J20 transgenic mice coincides with the deposition of Aβ plaques. These observations suggest that the Aβ trimers, hexamers, dodecamers, and related assemblies may be associated with presymptomatic neurodegeneration, while Aβ dimers are more closely associated with fibril formation and plaque deposition during symptomatic Alzheimer's disease.[16−20]

The approach of isolating and characterizing Aβ oligomers has not provided any high-resolution structures of Aβ oligomers. Techniques such as SDS-PAGE, TEM, and AFM have only provided information about the molecular weights, sizes, morphologies, and stoichiometry of Aβ oligomers. High-resolution structural studies of Aβ have primarily focused on Aβ fibrils and Aβ monomers. Solid-state NMR spectroscopy studies of Aβ fibrils revealed that Aβ fibrils are generally composed of extended networks of in-register parallel β-sheets.[21−27] X-ray crystallographic studies using fragments of Aβ have provided additional information about how Aβ fibrils pack.[28,29] Solution-phase NMR and solid-state NMR have been used to study the structures of the Aβ monomers within oligomeric assemblies.[30−35] A major finding from these studies is that oligomeric assemblies of Aβ are primarily composed of antiparallel β-sheets. Many of these studies have reported the monomer subunit as adopting a β-hairpin conformation, in which the hydrophobic central and C-terminal regions form an antiparallel β-sheet.

In 2008, Hoyer et al. reported the NMR structure of an Aβ monomer bound to an artificial binding protein called an affibody (PDB 2OTK).[36] The structure revealed that monomeric Aβ forms a β-hairpin when bound to the affibody. This Aβ β-hairpin encompasses residues 17−37 and contains two β-strands comprising $Aβ_{17−24}$ and $Aβ_{30−37}$ connected by an $Aβ_{25−29}$ loop. Sequestering Aβ within the affibody prevents its fibrilization and reduces its neurotoxicity, providing evidence that the β-hairpin structure may contribute to the ability of Aβ to form neurotoxic oligomers. In a related study, Sandberg et al. constrained Aβ in a β-hairpin conformation by mutating residues A_{21} and A_{30} to cysteine and forming an intramolecular disulfide bond.[37,38] Locking Aβ into a β-hairpin structure resulted in the formation Aβ oligomers, which were observed by size exclusion chromatography (SEC) and SDS-PAGE. The oligomers with a molecular weight of ∼100 kDa that were isolated by SEC were toxic toward neuronally derived SH-SY5Y cells. This study provides evidence for the role of β-hairpin structure in Aβ oligomerization and neurotoxicity.

Inspired by these β-hairpin structures, our laboratory developed a macrocyclic β-sheet peptide derived from $Aβ_{17−36}$ designed to mimic an Aβ β-hairpin and reported its X-ray crystallographic structure.[39] This peptide (peptide **1**) consists of two β-strands comprising $Aβ_{17−23}$ and $Aβ_{30−36}$ covalently linked by two δ-linked ornithine (^{δ}Orn) β-turn mimics.[40] The ^{δ}Orn that connects residues D_{23} and A_{30} replaces the $Aβ_{24−29}$ loop. The ^{δ}Orn that connects residues L_{17} and V_{36} enforces β-hairpin structure. We incorporated an *N*-methyl group at position G_{33} to prevent uncontrolled aggregation and precipitation of the peptide.[41] To improve the solubility of the peptide we replaced M_{35} with the hydrophilic isostere of methionine, ornithine (α-linked) (Figure 1B). The X-ray crystallographic structure of peptide **1** reveals that it folds to form a β-hairpin that assembles to form trimers and that the trimers further assemble to form hexamers and dodecamers.

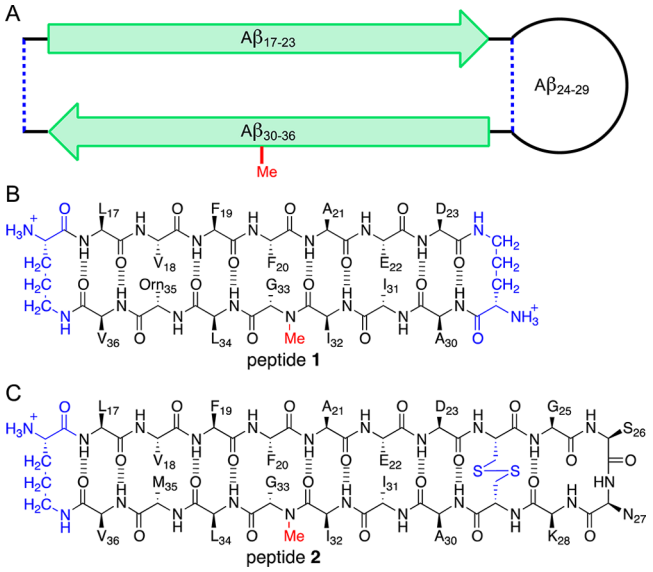

Figure 1. (A) Cartoon illustrating the design of peptides **1** and **2** and their relationship to an $Aβ_{17−36}$ β-hairpin. (B) Chemical structure of peptide **1** illustrating $Aβ_{17−23}$ and $Aβ_{30−36}$, M35Orn, the *N*-methyl group, and the δ-linked ornithine turns. (C) Chemical structure of peptide **2** illustrating $Aβ_{17−36}$, the *N*-methyl group, the disulfide bond across positions 24 and 29, and the δ-linked ornithine turn.

Our design of peptide **1** omitted the $Aβ_{24−29}$ loop. To visualize the $Aβ_{24−29}$ loop, we performed replica-exchange molecular dynamics (REMD) simulations on $Aβ_{17−36}$ using the X-ray crystallographic coordinates of $Aβ_{17−23}$ and $Aβ_{30−36}$ from peptide **1**.[39] These studies provided a working model for a trimer of $Aβ_{17−36}$ β-hairpins and demonstrated that the trimer should be capable of accommodating the $Aβ_{24−29}$ loop.

In the current study we set out to restore the $Aβ_{24−29}$ loop, reintroduce the methionine residue at position 35, and determine the X-ray crystallographic structures of oligomers that form. We designed peptide **2** as a homologue of peptide **1** that embodies these ideas. Peptide **2** contains a methionine residue at position 35 and an $Aβ_{24−29}$ loop with residues 24 and 29 (Val and Gly) mutated to cysteine and linked by a disulfide bond (Figure 1C). Here, we describe the development of peptide **2** and report the X-ray crystallographic structures of the trimer, dodecamer, and annular pore observed within the crystal structure.

RESULTS

1. Development of Peptide 2. We developed peptide **2** from peptide **1** by an iterative process, in which we first attempted to restore the $Aβ_{24−29}$ loop without a disulfide linkage. We envisioned peptide **3** as a homologue of peptide **1** with the $Aβ_{24−29}$ loop in place of the ^{δ}Orn that connects D_{23} and A_{30} and *p*-iodophenylalanine (F^{I}) in place of F_{19}. We routinely use *p*-iodophenylalanine to determine the X-ray crystallographic phases. After determining the X-ray crystallo-

DOI: 10.1021/jacs.6b01332
J. Am. Chem. Soc. 2016, 138, 4634−4642

graphic structure of the *p*-iodophenylalanine variant we attempt to determine the structure of the native phenylalanine compound by isomorphous replacement.[42] Upon synthesizing peptide **3**, we found that it formed an amorphous precipitate in most crystallization conditions screened and failed to afford crystals in any condition.

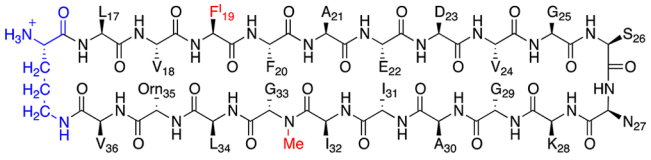

peptide **3**

We postulate that the loss of the $^{\delta}$Orn constraint leads to conformational heterogeneity that prevents peptide **3** from crystallizing. To address this issue, we next incorporated a disulfide bond between residues 24 and 29 as a conformational constraint that serves as a surrogate for $^{\delta}$Orn. We designed peptide **4** to embody this idea, mutating Val_{24} and Gly_{29} to cysteine and forming an interstrand disulfide linkage. We mutated these residues because they occupy the same position as the $^{\delta}$Orn that connects D_{23} and A_{30} in peptide **1**. Residues V_{24} and G_{29} form a non-hydrogen-bonded pair, which can readily accommodate disulfide linkages in antiparallel β-sheets. Disulfide bonds across non-hydrogen-bonded pairs stabilize β-hairpins, while disulfide bonds across hydrogen-bonded pairs do not.[43] Although the disulfide bond between positions 24 and 29 helps stabilize the β-hairpin, it does not alter the charge or substantially change the hydrophobicity of the $A\beta_{17-36}$ β-hairpin. We were gratified to find that peptide **4** afforded crystals suitable for X-ray crystallography. As the next step in the iterative process, we determined the X-ray crystallographic structure of this peptide (PDB 5HOW).

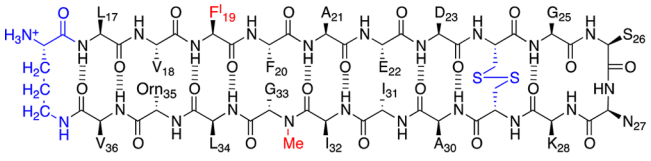

peptide **4**

After determining the X-ray crystallographic structure of peptide **4** we reintroduced the native phenylalanine at position 19 and the methionine at position 35 to afford peptide **2**. We completed the iterative process—from **1** to **3** to **4** to **2**—by successfully determining the X-ray crystallographic structure of peptide **2** (PDB 5HOX and 5HOY). The following sections describe the synthesis of peptides **2**–**4** and the X-ray crystallographic structure of peptide **2**.

2. Synthesis of Peptides 2–4. We synthesized peptides **2**–**4** by similar procedures to those we have developed for other macrocyclic peptides.[39,44,45] Our laboratory routinely prepares macrocyclic peptides by solid-phase synthesis of the corresponding linear peptide on 2-chlorotrityl resin, followed by cleavage of the protected linear peptide from the resin, solution-phase macrolactamization, and deprotection of the resulting macrocyclic peptide. In synthesizing peptides **2** and **4** we formed the disulfide linkage after macrolactamization and deprotection of the acid-labile side chain protecting groups. We used acid-stable Acm-protected cysteine residues at positions 24 and 29 and removed the Acm groups by oxidation with I_2 in aqueous acetic acid to afford the disulfide linkage. Peptides **2**–**4** were purified by RP-HPLC.

3. Crystallization, X-ray Crystallographic Data Collection, Data Processing, and Structure Determination of Peptides 2 and 4. We screened crystallization conditions for peptide **4** in a 96-well-plate format using three different Hampton Research crystallization kits (Crystal Screen, Index, and PEG/Ion) with three ratios of peptide and mother liquor per condition (864 experiments). Peptide **4** afforded crystals in a single set of conditions containing HEPES buffer and Jeffamine M-600—the same crystallization conditions that afforded crystals of peptide **1**. Peptide **2** also afforded crystals in these conditions. We further optimized these conditions to rapidly (~72 h) yield crystals suitable for X-ray crystallography. The optimized conditions consist of 0.1 M HEPES at pH 6.4 with 31% Jeffamine M-600 for peptide **4** and 0.1 M HEPES pH 7.1 with 29% Jeffamine M-600 for peptide **2**.

Crystal diffraction data for peptides **4** and **2** were collected in-house with a Rigaku MicroMax 007HF X-ray diffractometer at 1.54 Å wavelength. Crystal diffraction data for peptide **2** were also collected at the Advanced Light Source at Lawrence Berkeley National Laboratory with a synchrotron source at 1.00 Å wavelength to achieve higher resolution. Data from peptides **4** and **2** suitable for refinement at 2.30 Å were obtained from the diffractometer; data from peptide **2** suitable for refinement at 1.90 Å were obtained from the synchrotron.

Data for peptides **4** and **2** were scaled and merged using XDS.[46] Phases for peptide **4** were determined by single-wavelength anomalous diffraction (SAD) phasing by using the coordinates of the iodine anomalous signal from *p*-iodophenylalanine. Phases for peptide **2** were determined by isomorphous replacement of peptide **4**. The structures of peptides **2** and **4** were solved and refined in the $P6_122$ space group. Coordinates for hydrogens were generated by phenix.refine during refinement. The asymmetric unit of each peptide consists of six monomers, arranged as two trimers. Peptides **2** and **4** form morphologically identical structures and assemblies in the crystal lattice.

4. X-ray Crystallographic Structure of Peptide 2 and the Oligomers It Forms. The X-ray crystallographic structure of peptide **2** reveals that it folds to form a twisted β-hairpin comprising two β-strands connected by a loop (Figure 2A).

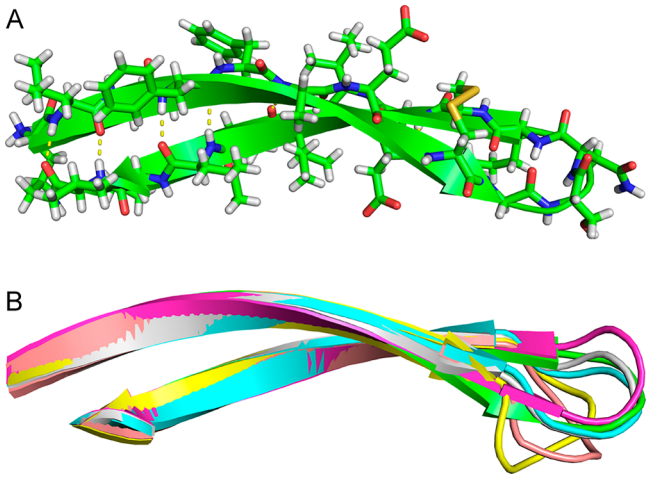

Figure 2. X-ray crystallographic structure of peptide **2** (PDB 5HOX, synchrotron data set). (A) X-ray crystallographic structure of a representative β-hairpin monomer formed by peptide **2**. (B) Overlay of the six β-hairpin monomers in the asymmetric unit. The β-hairpins are shown as cartoons to illustrate the differences in the $A\beta_{25-28}$ loops.

DOI: 10.1021/jacs.6b01332
J. Am. Chem. Soc. 2016, 138, 4634–4642

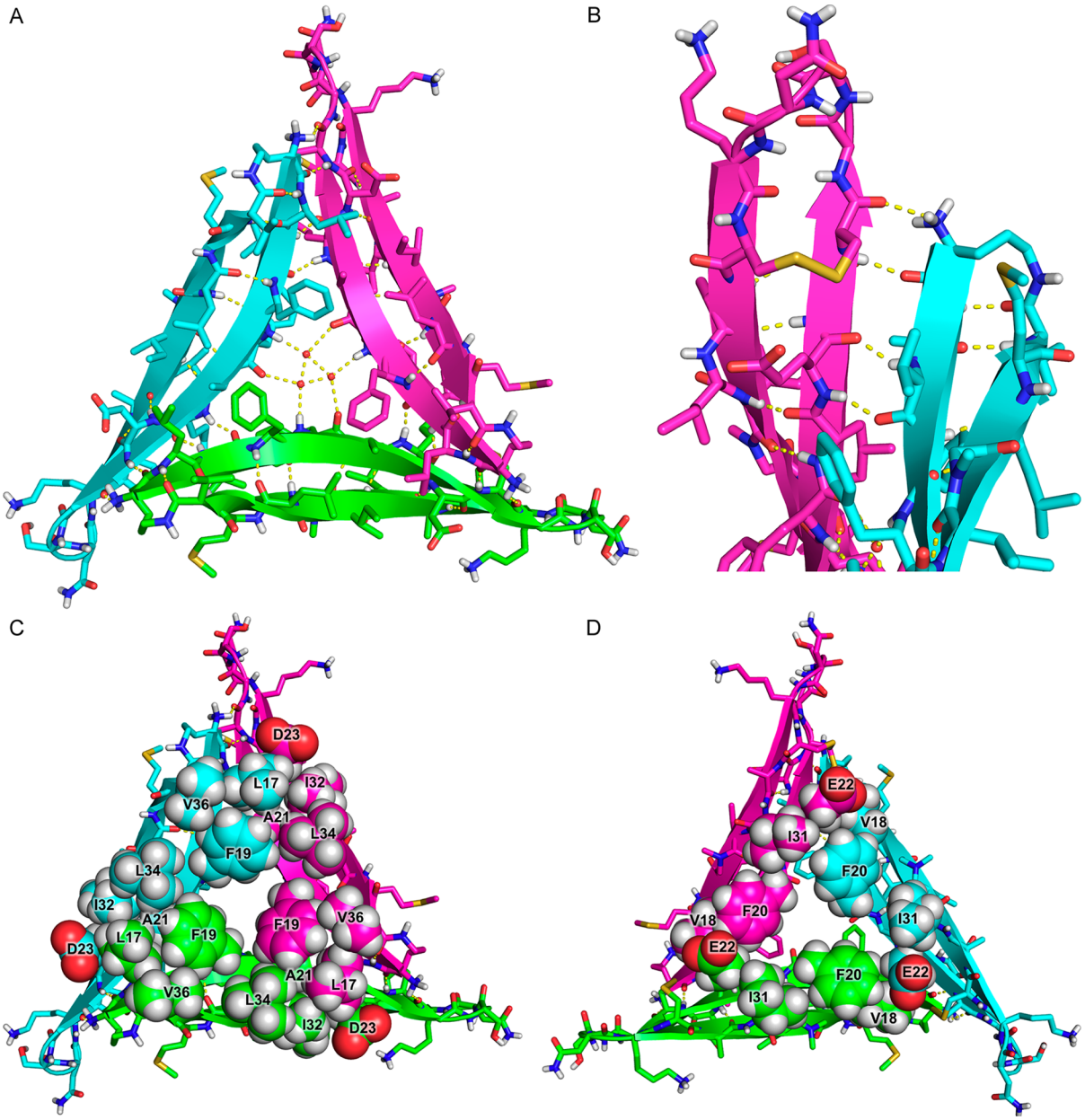

Figure 3. X-ray crystallographic structure of the trimer formed by peptide **2**. (A) Triangular trimer. The three water molecules in the center hole of the trimer are shown as spheres. (B) Detailed view of the intermolecular hydrogen bonds between the main chains of V_{18} and E_{22} and $^{\delta}$Orn and C_{24}, at the three corners of the triangular trimer. (C) The F_{19} face of the trimer, with key side chains shown as spheres. (D) The F_{20} face of the trimer, with key side chains as spheres.

Eight residues make up each surface of the β-hairpin: L_{17}, F_{19}, A_{21}, D_{23}, A_{30}, I_{32}, L_{34}, and V_{36} make up one surface; V_{18}, F_{20}, E_{22}, C_{24}, C_{29}, I_{31}, G_{33}, and M_{35} make up the other surface. The β-strands of the monomers in the asymmetric unit are virtually identical, differing primarily in rotamers of F_{20}, E_{22}, C_{24}, C_{29}, I_{31}, and M_{35} (Figure S1). The disulfide linkages suffered radiation damage under synchrotron radiation.[47,48] We refined three of the β-hairpins with intact disulfide linkages and three with thiols to represent cleaved disulfide linkages in the synchrotron data set (PDB 5HOX). No evidence for cleavage of the disulfides was observed in the refinement of the data set collected on the X-ray diffractometer, and we refined all disulfide linkages as intact (PDB 5HOY).

The Aβ_{25-28} loops of the six monomers within the asymmetric unit vary substantially in backbone geometry and side chain rotamers (Figures 2B and S1). The electron density for the loops is weak and diffuse compared to the electron density for the β-strands. The B values for the loops are large, indicating that the loops are dynamic and not well ordered. Thus, the differences in backbone geometry and side chain rotamers among the loops are likely of little significance and should be interpreted with caution.

Peptide **2** assembles into oligomers similar in morphology to those formed by peptide **1**. Like peptide **1**, peptide **2** forms a triangular trimer, and four trimers assemble to form a dodecamer. In the higher-order assembly of the dodecamers formed by peptide **2** a new structure emerges, not seen in peptide **1**, an annular pore consisting of five dodecamers.

Trimer. Peptide **2** forms a trimer, much like that which we observed previously for peptide **1**, in which three β-hairpins

DOI: 10.1021/jacs.6b01332
J. Am. Chem. Soc. 2016, 138, 4634−4642

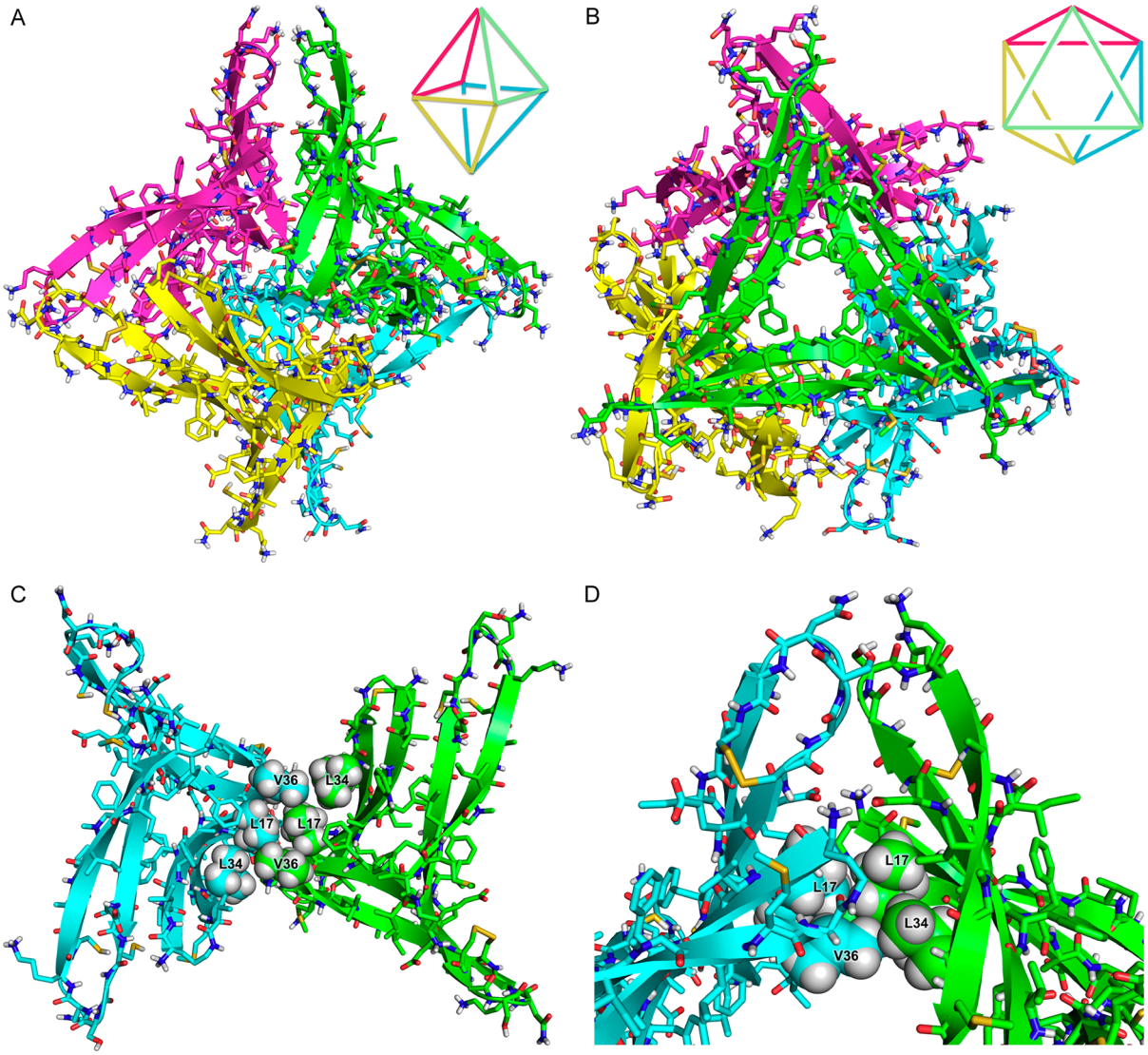

Figure 4. X-ray crystallographic structure of the dodecamer formed by peptide **2**. (A) View of the dodecamer that illustrates the octahedral shape. (B) View of the dodecamer that illustrates the tetrahedral arrangement of the four trimers that comprise the dodecamer. (C) View of two trimer subunits from inside the cavity of the dodecamer. Residues L_{17}, L_{34}, and V_{36} are shown as spheres, illustrating the hydrophobic packing that occurs at the six vertices of the dodecamer. (D) Detailed view of one of the six vertices of the dodecamer.

assemble to form an equilateral triangle (Figure 3A). The trimer maintains all of the same stabilizing contacts as those of peptide **1**. Hydrogen bonding and hydrophobic interactions between residues on the β-strands comprising Aβ_{17-23} and Aβ_{30-36} stabilize the core of the trimer. The disulfide bonds between residues 24 and 29 are adjacent to the structural core of the trimer and do not make any substantial intermolecular contacts. Two crystallographically distinct trimers comprise the peptide portion of the asymmetric unit. The two trimers are almost identical in structure, differing slightly among side chain rotamers and loop conformations.

A network of 18 intermolecular hydrogen bonds helps stabilize the trimer. At the corners of the trimer, the pairs of β-hairpin monomers form four hydrogen bonds: two between the main chains of V_{18} and E_{22} and two between $^{\delta}$Orn and the main chain of C_{24} (Figure 3B). Three ordered water molecules fill the hole in the center of the trimer, hydrogen bonding to each other and to the main chain of F_{20} (Figure 3A).

Hydrophobic contacts between residues at the three corners of the trimer, where the β-hairpins meet, further stabilize the trimer. At each corner, the side chains of residues L_{17}, F_{19}, and V_{36} of one β-hairpin pack against the side chains of residues A_{21}, I_{32}, L_{34}, and also D_{23} of the adjacent β-hairpin to create a hydrophobic cluster (Figure 3C). The three hydrophobic clusters create a large hydrophobic surface on one face of the trimer. The other face of the trimer displays a smaller hydrophobic surface, which includes the side chains of residues V_{18}, F_{20}, and I_{31} of the three β-hairpins (Figure 3D). In subsequent discussion, we designate the former surface the "F_{19} face" and the latter surface the "F_{20} face".

Dodecamer. Four trimers assemble to form a dodecamer. The four trimers arrange in a tetrahedral fashion, creating a central cavity inside the dodecamer. Because each trimer is triangular, the resulting arrangement resembles an octahedron. Each of the 12 β-hairpins constitutes an edge of the octahedron, and the triangular trimers occupy four of the eight faces of the octahedron. Figure 4A illustrates the octahedral shape of the dodecamer. Figure 4B illustrates the tetrahedral arrangement of the four trimers.

DOI: 10.1021/jacs.6b01332
J. Am. Chem. Soc. 2016, 138, 4634−4642

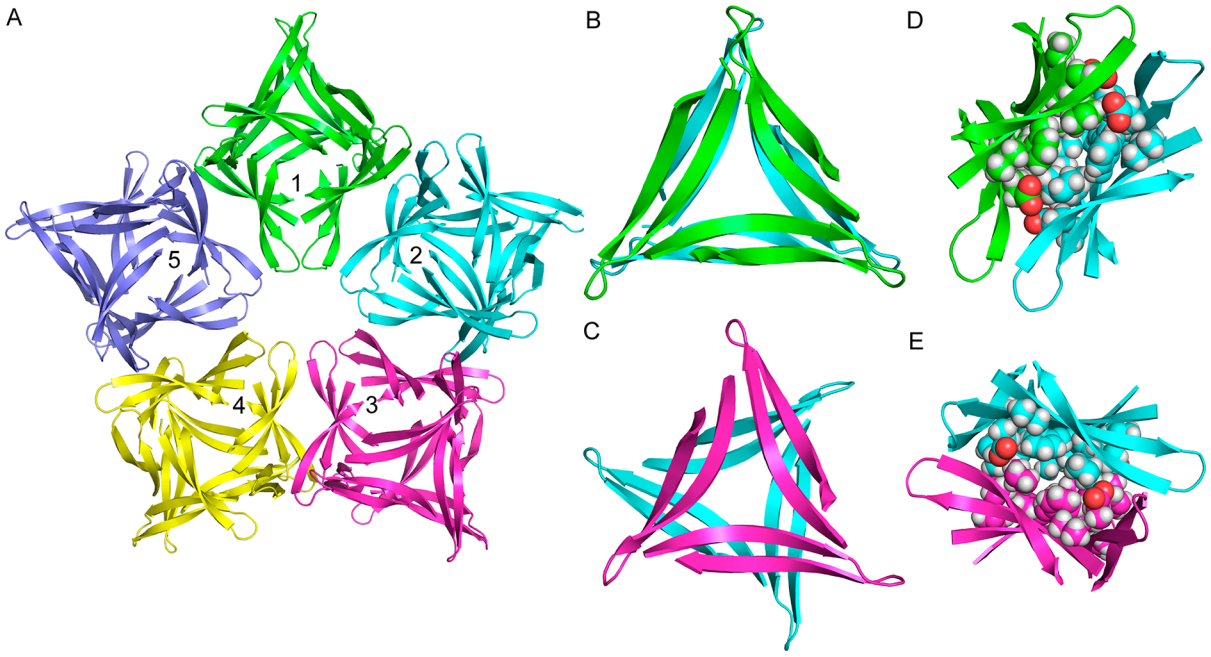

Figure 5. X-ray crystallographic structure of the annular pore formed by peptide **2**. (A) Annular porelike structure illustrating the relationship of the five dodecamers that form the pore (top view). (B) Eclipsed interface between dodecamers 1 and 2 (side view). The same eclipsed interface also occurs between dodecamers 1 and 5 and 3 and 4. (C) Staggered interface between dodecamers 2 and 3 (side view). The same staggered interface also occurs between dodecamers 4 and 5. (D) Eclipsed interface between dodecamers 1 and 5 (top view). Residues F_{20}, I_{31}, and E_{22} are shown as spheres to detail the hydrophobic packing. (E) Staggered interface between dodecamers 2 and 3 (top view). Residues F_{20}, I_{31}, and E_{22} are shown as spheres to detail the hydrophobic packing.

The F_{19} faces of the trimers line the interior of the dodecamer. At the six vertices, hydrophobic packing between the side chains of L_{17}, L_{34}, and V_{36} helps stabilize the dodecamer (Figures 4C and D). Salt bridges between the side chains of D_{23} and $^{\delta}$Orn at the vertices further stabilize the dodecamer.[49] Each of the six vertices includes two Aβ_{25-28} loops that extend past the core of the dodecamer without making any substantial intermolecular contacts. The exterior of the dodecamer displays four F_{20} faces (Figure S3). In the crystal lattice, each F_{20} face of one dodecamer packs against an F_{20} face of another dodecamer. Although the asymmetric unit comprises half a dodecamer, the crystal lattice may be thought of as being built of dodecamers.

The electron density map for the X-ray crystallographic structure of peptide **2** has long tubes of electron density inside the central cavity of the dodecamer. The shape and length of the electron density is consistent with the structure of Jeffamine M-600, which is an essential component of the crystallization conditions. Jeffamine M-600 is a polypropylene glycol derivative with a 2-methoxyethoxy unit at one end and a 2-aminopropyl unit at the other end. Its average molecular weight is about 600 Da, which corresponds to nine propylene glycol units. Although Jeffamine M-600 is a heterogeneous mixture with varying chain lengths and stereochemistry, we modeled a single stereoisomer with nine propylene glycol units (n = 9) to fit the electron density. The Jeffamine M-600 appears to stabilize the dodecamer by occupying the central cavity and making hydrophobic contacts with residues lining the cavity (Figure S3). In a dodecamer formed by full-length Aβ, the hydrophobic *C*-terminal residues (Aβ_{37-40} or Aβ_{37-42}) might play a similar role in filling the dodecamer and thus create a packed hydrophobic core within the central cavity of the dodecamer.

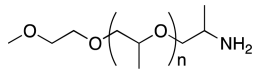

Jeffamine M-600

Annular Pore. Five dodecamers assemble to form an annular porelike structure (Figure 5A). Hydrophobic packing between the F_{20} faces of trimers displayed on the outer surface of each dodecamer stabilizes the porelike assembly. Two morphologically distinct interactions between trimers occur at the interfaces of the five dodecamers: one in which the trimers are eclipsed (Figure 5B), and one in which the trimers are staggered (Figure 5C). Hydrophobic packing between the side chains of F_{20}, I_{31}, and E_{22} stabilizes these interfaces (Figure 5D and E). The annular pore contains three eclipsed interfaces and two staggered interfaces. The eclipsed interfaces occur between dodecamers 1 and 2, 1 and 5, and 3 and 4, as shown in Figure 5A. The staggered interfaces occur between dodecamers 2 and 3 and 4 and 5. The annular pore is not completely flat, instead, adopting a slightly puckered shape, which accommodates the eclipsed and staggered interfaces. Ten Aβ_{25-28} loops from the vertices of the five dodecamers line the hole in the center of the pore. The hydrophilic side chains of S_{26}, N_{27}, and K_{28} decorate the hole.

The annular pore is comparable in size to other large protein assemblies.[50] The outer diameter is ~11−12 nm. The diameter of the hole in the center of the pore is ~2 nm. The thickness of the pore is ~5 nm, which is comparable to that of a lipid bilayer membrane.[51] It is important to note that the annular pore formed by peptide **2** is not a discrete unit in the crystal lattice. Rather, the crystal lattice is composed of conjoined annular pores in which all four F_{20} faces on the surface of each dodecamer contact F_{20} faces on other dodecamers (Figure S4). The crystal lattice shows how the dodecamers can further assemble to form larger structures. Each dodecamer may be

DOI: 10.1021/jacs.6b01332
J. Am. Chem. Soc. 2016, 138, 4634−4642

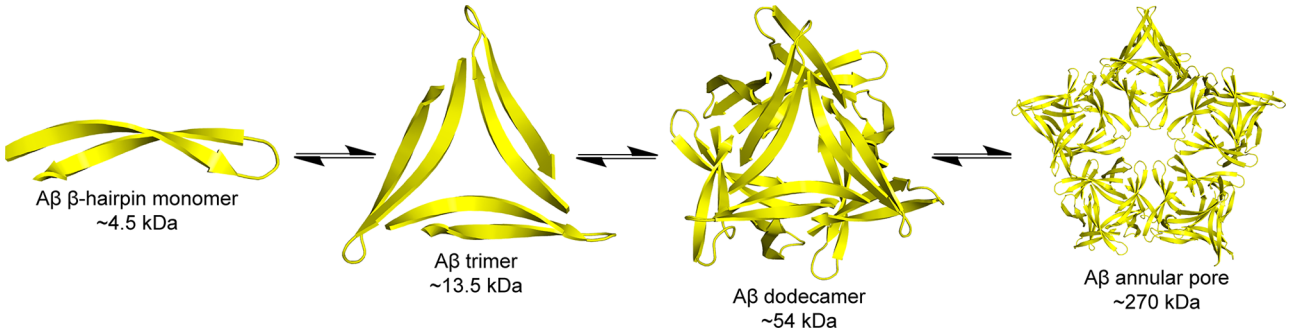

Figure 6. Model for the hierarchical assembly of an Aβ β-hairpin into a trimer, dodecamer, and annular pore based on the crystallographic assembly of peptide **2**. Monomeric Aβ folds to form a β-hairpin in which the hydrophobic central and *C*-terminal regions form an antiparallel β-sheet. Three β-hairpin monomers assemble to form a triangular trimer. Four triangular trimers assemble to form a dodecamer. Five dodecamers assemble to form an annular pore. The molecular weights shown correspond to an $A\beta_{42}$ monomer (~4.5 kDa), an $A\beta_{42}$ trimer (~13.5 kDa), an $A\beta_{42}$ dodecamer (~54 kDa), and an $A\beta_{42}$ annular pore composed of five dodecamers (~270 kDa).

thought of as a tetravalent building block with the potential to assemble on all four faces to form higher-order supramolecular assemblies.

DISCUSSION

The X-ray crystallographic study of peptide **2** described here provides high-resolution structures of oligomers formed by an $A\beta_{17-36}$ β-hairpin. The crystallographic assembly of peptide **2** into a trimer, dodecamer, and annular pore provides a model for the assembly of the full-length Aβ peptide to form oligomers. In this model Aβ folds to form a β-hairpin comprising the hydrophobic central and *C*-terminal regions. Three β-hairpins assemble to form a trimer, and four trimers assemble to form a dodecamer. The dodecamers further assemble to form an annular pore (Figure 6).

The model put forth in Figure 6 is consistent with the current understanding of endogenous Aβ oligomerization and explains at atomic resolution many key observations about Aβ oligomers. Two general types of endogenous Aβ oligomers have been observed: Aβ oligomers that occur on a pathway to fibrils, or "fibrillar oligomers", and Aβ oligomers that evade a fibrillar fate, or "nonfibrillar oligomers".[52−54] Fibrillar oligomers accumulate in Alzheimer's disease later than nonfibrillar oligomers and coincide with the deposition of plaques. Nonfibrillar oligomers accumulate early in Alzheimer's disease before plaque deposition.

Fibrillar and nonfibrillar oligomers have structurally distinct characteristics, which are reflected in their reactivity with the fibril-specific OC antibody and the oligomer-specific A11 antibody.[55] Fibrillar oligomers are recognized by the OC antibody but not the A11 antibody, whereas nonfibrillar oligomers are recognized by the A11 antibody but not the OC antibody. These criteria have been used to classify the Aβ oligomers that accumulate *in vivo*. Aβ dimers have been classified as fibrillar oligomers, whereas Aβ trimers, Aβ*56, and APFs have been classified as nonfibrillar oligomers.

Larson and Lesné proposed a model for the endogenous production of nonfibrillar oligomers that explains these observations.[53] In this model, folded Aβ monomer assembles into a trimer, the trimer further assembles into hexamers and dodecamers, and the dodecamers further assemble to form annular protofibrils. The hierarchical assembly of peptide **2** is consistent with this model; and the trimer, dodecamer, and annular pore formed by peptide **2** may share similarities to the trimers, Aβ*56, and APFs observed *in vivo*. At this point, we can only speculate whether the trimer and dodecamer formed by peptide **2** share structural similarities to Aβ trimers and Aβ*56, as little is known about the structure of Aβ trimers and Aβ*56.

The crystallographically observed annular pore formed by peptide **2** is morphologically similar to the APFs formed by full-length Aβ. The annular pore formed by peptide **2** is comparable in size to the APFs prepared *in vitro* or isolated from Alzheimer's brains (Figure 7 and Table 1). The varying sizes

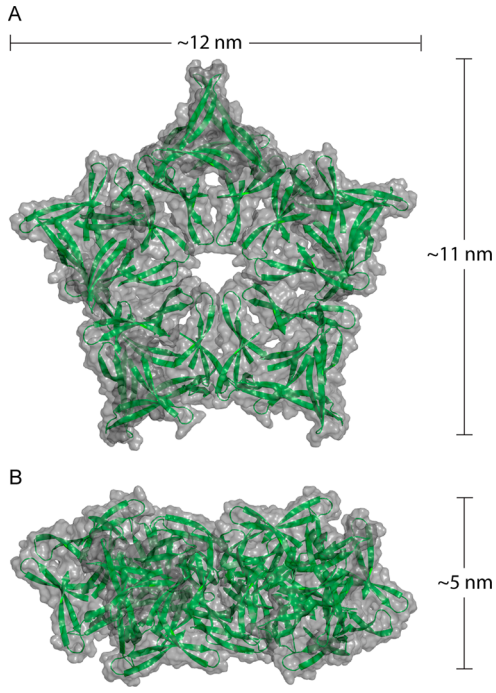

Figure 7. Surface views of the annular pore formed by peptide **2**. (A) Top view. (B) Side view.

of APFs formed by full-length Aβ might result from differences in the number of oligomer subunits comprising each APF. Although the annular pore formed by peptide **2** contains five dodecamer subunits, pores containing fewer or more subunits can easily be envisioned. The dodecamers that comprise the annular pore exhibit two modes of assembly—eclipsed interactions and staggered interactions between the F_{20} faces of trimers within dodecamers. These two modes of assembly

DOI: 10.1021/jacs.6b01332
J. Am. Chem. Soc. 2016, 138, 4634−4642

Table 1. Annular Pores Formed by Aβ and Peptide 2

annular pore source	outer diameter	inner diameter	observation method
peptide **2**	∼11−12 nm	∼2 nm	X-ray crystallography
synthetic Aβ[6]	7−10 nm	1.5−2 nm	TEM
synthetic Aβ[7]	16 nm	not reported	AFM
synthetic Aβ[8]	8−25 nm	not reported	TEM
Alzheimer's brain[10]	11−14 nm	2.5−4 nm	TEM

might reflect a dynamic interaction between dodecamers, which could permit assemblies of more dodecamers into larger annular pores.

Dot blot analysis shows that peptide **2** is reactive toward the A11 antibody (Figure S5). This reactivity suggests that peptide **2** forms oligomers in solution that share structural similarities to the nonfibrillar oligomers formed by full-length Aβ. Further studies are needed to elucidate the species that peptide **2** forms in solution and to study their biological properties. This is an active area of research in our laboratory. Preliminary attempts to study these species by SEC and SDS-PAGE have not provided a clear measure of the structures formed in solution. The difficulty in studying the oligomers formed in solution may reflect the propensity of the dodecamer to assemble on all four F_{20} faces.

The X-ray crystallographic structure and A11 reactivity of peptide **2** support the model proposed by Larsen and Lesné and suggest that β-hairpins constitute a fundamental building block for nonfibrillar oligomers.[53] What makes β-hairpins special is that three β-hairpins can nestle together to form trimers, stabilized by a network of hydrogen bonds and hydrophobic interactions. This mode of assembly is not unique to Aβ. The foldon domain of bacteriophage T4 fibritin is composed of three β-hairpins that assemble into a triangular trimer similar to the triangular trimer formed by peptide **2**.[56] Additionally, our research group has observed a similar assembly of a β-hairpin peptide derived from β_2-microglobulin.[44]

CONCLUSION

Although we began these studies with a relatively simple hypothesis—that the trimers and dodecamers formed by peptide **1** could accommodate the $A\beta_{24-29}$ loop—an even more exciting finding has emerged—that the dodecamers can assemble to form annular pores. This finding could not have been anticipated from the X-ray crystallographic structure of peptide **1** and reveals a new level of hierarchical assembly that recapitulates micrographic observations of annular protofibrils. The crystallographically observed dodecamer, in turn, recapitulates the observation of Aβ*56, which appears to be a dodecamer of Aβ. The crystallographically observed trimer recapitulates the Aβ trimers that are observed even before the onset of symptoms in Alzheimer's disease.

Our approach of constraining $A\beta_{17-36}$ into a β-hairpin conformation and blocking aggregation with an *N*-methyl group has allowed us to crystallize a large fragment of what is generally considered to be an uncrystallizable peptide. We believe this iterative, "bottom up" approach of identifying the minimal modification required to crystallize Aβ peptides will ultimately allow larger fragments of Aβ to be crystallized, thus providing greater insights into the structures of Aβ oligomers.

ASSOCIATED CONTENT

Supporting Information

The Supporting Information is available free of charge on the ACS Publications website at DOI: 10.1021/jacs.6b01332.

Procedures for the synthesis and crystallization of peptides **2**−**4**; details of X-ray crystallographic data collection, processing, and refinement; procedure and data for dot blot analysis (PDF)

Crystallographic coordinates of peptide **2** deposited into the Protein Data Bank (PDB) with code 5HOX (data collected on a synchrotron at 1.00 Å wavelength) (PDB)

Crystallographic coordinates of peptide **2** deposited into the Protein Data Bank (PDB) with code 5HOY (data collected on an X-ray diffractometer at 1.54 Å wavelength) (PDB)

Crystallographic coordinates of peptide **4** deposited into the Protein Data Bank (PDB) with code 5HOW (PDB)

Crystallographic coordinates of the dodecamer formed by peptide **2** (PDB)

Crystallographic coordinates of the annular pore formed by peptide **2** (PDB)

Crystallographic data for 5HOW (CIF)

Crystallographic data for 5HOX (CIF)

Crystallographic data for 5HOY (CIF)

AUTHOR INFORMATION

Corresponding Author

*jsnowick@uci.edu.

Notes

The authors declare no competing financial interest.

ACKNOWLEDGMENTS

We thank Dr. Huiying Li and Mr. Ricardo Albay for helpful advice and assistance, Dr. Charles G. Glabe for a gift of A11 antibody, the National Institutes of Health (NIH) National Institute of General Medical Sciences (NIGMS) for funding (Grant GM097562), and the Berkeley Center for Structural Biology (BCSB) beamlines of the Advanced Light Source (ALS) for synchrotron data collection. The BCSB is supported in part by the NIH, NIGMS, and the Howard Hughes Medical Institute. The ALS is supported by the Director, Office of Science, Office of Basic Energy Sciences, of the U.S. Department of Energy under Contract No. DE-AC02-05CH11231.

REFERENCES

(1) Benilova, I.; Karran, E.; De Strooper, B. *Nat. Neurosci.* **2012**, *15*, 349−357.

(2) Lesné, S.; Koh, M. T.; Kotilinek, L.; Kayed, R.; Glabe, C. G.; Yang, A.; Gallagher, M.; Ashe, K. H. *Nature* **2006**, *440*, 352−357.

(3) Lesné, S. E.; Sherman, M. A.; Grant, M.; Kuskowski, M.; Schneider, J. A.; Bennett, D. A.; Ashe, K. H. *Brain* **2013**, *136*, 1383−1398.

(4) Hafner, J. H.; Cheung, C. L.; Woolley, A. T.; Lieber, C. M. *Prog. Biophys. Mol. Biol.* **2001**, *77*, 73−110.

(5) Lin, H.; Bhatia, R.; Lal, R. *FASEB J.* **2001**, *15*, 2433−2444.

(6) Lashuel, H. A.; Hartley, D.; Petre, B. M.; Walz, T.; Lansbury, P. T., Jr. *Nature* **2002**, *418*, 291−292.

(7) Quist, A.; Doudevski, I.; Lin, H.; Azimova, R.; Ng, D.; Frangione, B.; Kagan, B.; Ghiso, J.; Lal, R. *Proc. Natl. Acad. Sci. U. S. A.* **2005**, *102*, 10427−10432.

(8) Kayed, R.; Pensalfini, A.; Margol, L.; Sokolov, Y.; Sarsoza, F.; Head, E.; Hall, J.; Glabe, C. *J. Biol. Chem.* **2009**, *284*, 4230−4237.

DOI: 10.1021/jacs.6b01332
J. Am. Chem. Soc. 2016, 138, 4634−4642

(9) Kokubo, H.; Kayed, R.; Glabe, C. G.; Staufenbiel, M.; Saido, T. C.; Iwata, N.; Yamaguchi, H. *Int. J. Alzheimer's Dis.* **2009**, *2009*, 689285.
(10) Lasagna-Reeves, C. A.; Glabe, C. G.; Kayed, R. *J. Biol. Chem.* **2011**, *286*, 22122−22130.
(11) Roher, A. E.; Chaney, M. O.; Kuo, Y. M.; Webster, S. D.; Stine, W. B.; Haverkamp, L. J.; Woods, A. S.; Cotter, R. J.; Tuohy, J. M.; Krafft, G. A.; Bonnell, B. S.; Emmerling, M. R. *J. Biol. Chem.* **1996**, *271*, 20631−20635.
(12) McLean, C. A.; Cherny, R. A.; Fraser, F. W.; Fuller, S. J.; Smith, M. J.; Beyreuther, K.; Bush, A. I.; Masters, C. L. *Ann. Neurol.* **1999**, *46*, 860−866.
(13) McDonald, J. M.; Savva, G. M.; Brayne, C.; Welzel, A. T.; Forster, G.; Shankar, G. M.; Selkoe, D. J.; Ince, P. G.; Walsh, D. M. *Brain* **2010**, *133*, 1328−1341.
(14) Shankar, G. M.; Li, S.; Mehta, T. H.; Garcia-Munoz, A.; Shepardson, N. E.; Smith, I.; Brett, F. M.; Farrell, M. A.; Rowan, M. J.; Lemere, C. A.; Regan, C. M.; Walsh, D. M.; Sabatini, B. L.; Selkoe, D. J. *Nat. Med.* **2008**, *14*, 837−842.
(15) Jin, M.; Shepardson, N.; Yang, T.; Chen, G.; Walsh, D.; Selkoe, D. J. *Proc. Natl. Acad. Sci. U. S. A.* **2011**, *108*, 5819−5824.
(16) Mucke, L.; Masliah, E.; Yu, G. Q.; Mallory, M.; Rockenstein, E. M.; Tatsuno, G.; Hu, K.; Kholodenko, D.; Johnson-Wood, K.; McConlogue, L. *J. Neurosci.* **2000**, *20*, 4050−4058.
(17) Kawarabayashi, T.; Younkin, L. H.; Saido, T. C.; Shoji, M.; Ashe, K. H.; Younkin, S. G. *J. Neurosci.* **2001**, *21*, 372−381.
(18) Kawarabayashi, T.; Shoji, M.; Younkin, L. H.; Wen-Lang, L.; Dickson, D. W.; Murakami, T.; Matsubara, E.; Abe, K.; Ashe, K. H.; Younkin, S. G. *J. Neurosci.* **2004**, *24*, 3801−3809.
(19) Meilandt, W. J.; Cisse, M.; Ho, K.; Wu, T.; Esposito, L. A.; Scearce-Levie, K.; Cheng, I. H.; Yu, G. Q.; Mucke, L. *J. Neurosci.* **2009**, *29*, 1977−1986.
(20) Shankar, G. M.; Leissring, M. A.; Adame, A.; Sun, X.; Spooner, E.; Masliah, E.; Selkoe, D. J.; Lemere, C. A.; Walsh, D. M. *Neurobiol. Dis.* **2009**, *36*, 293−302.
(21) Benzinger, T. L.; Gregory, D. M.; Burkoth, T. S.; Miller-Auer, H.; Lynn, D. G.; Botto, R. E.; Meredith, S. C. *Proc. Natl. Acad. Sci. U. S. A.* **1998**, *95*, 13407−13412.
(22) Petkova, A. T.; Leapman, R. D.; Guo, Z.; Yau, W. M.; Mattson, M. P.; Tycko, R. *Science* **2005**, *307*, 262−265.
(23) Lührs, T.; Ritter, C.; Adrian, M.; Riek-Loher, D.; Bohrmann, B.; Döbeli, H.; Schubert, D.; Riek, R. *Proc. Natl. Acad. Sci. U. S. A.* **2005**, *102*, 17342−17347.
(24) Petkova, A. T.; Yau, W. M.; Tycko, R. *Biochemistry* **2006**, *45*, 498−512.
(25) Paravastu, A. K.; Petkova, A. T.; Tycko, R. *Biophys. J.* **2006**, *90*, 4618−4629.
(26) Lu, J. X.; Qiang, W.; Yau, W. M.; Schwieters, C. D.; Meredith, S. C.; Tycko, R. *Cell* **2013**, *154*, 1257−1268.
(27) Xiao, Y.; Ma, B.; McElheny, D.; Parthasarathy, S.; Long, F.; Hoshi, M.; Nussinov, R.; Ishii, Y. *Nat. Struct. Mol. Biol.* **2015**, *22*, 499−505.
(28) Sawaya, M. R.; Sambashivan, S.; Nelson, R.; Ivanova, M. I.; Sievers, S. A.; Apostol, M. I.; Thompson, M. J.; Balbirnie, M.; Wiltzius, J. J.; McFarlane, H. T.; Madsen, A. Ø.; Riekel, C.; Eisenberg, D. *Nature* **2007**, *447*, 453−457.
(29) Colletier, J. P.; Laganowsky, A.; Landau, M.; Zhao, M.; Soriaga, A. B.; Goldschmidt, L.; Flot, D.; Cascio, D.; Sawaya, M. R.; Eisenberg, D. *Proc. Natl. Acad. Sci. U. S. A.* **2011**, *108*, 16938−16943.
(30) Yu, L.; Edalji, R.; Harlan, J. E.; Holzman, T. F.; Lopez, A. P.; Labkovsky, B.; Hillen, H.; Barghorn, S.; Ebert, U.; Richardson, P. L.; Miesbauer, L.; Solomon, L.; Bartley, D.; Walter, K.; Johnson, R. W.; Hajduk, P. J.; Olejniczak, E. T. *Biochemistry* **2009**, *48*, 1870−1877.
(31) Scheidt, H. A.; Morgado, I.; Huster, D. *J. Biol. Chem.* **2012**, *287*, 22822−22826.
(32) Doi, T.; Masuda, Y.; Irie, K.; Akagi, K.; Monobe, Y.; Imazawa, T.; Takegoshi, K. *Biochem. Biophys. Res. Commun.* **2012**, *428*, 458−462.
(33) Gu, L.; Liu, C.; Guo, Z. *J. Biol. Chem.* **2013**, *288*, 18673−18683.
(34) Tay, W. M.; Huang, D.; Rosenberry, T. L.; Paravastu, A. K. *J. Mol. Biol.* **2013**, *425*, 2494−2508.
(35) Potapov, A.; Yau, W.-M.; Ghirlando, R.; Thurber, K. R.; Tycko, R. *J. Am. Chem. Soc.* **2015**, *137*, 8294−8307.
(36) Hoyer, W.; Grönwall, C.; Jonsson, A.; Ståhl, S.; Härd, T. *Proc. Natl. Acad. Sci. U. S. A.* **2008**, *105*, 5099−6104.
(37) Sandberg, A.; Luheshi, L. M.; Söllvander, S.; Pereira de Barros, T.; Macao, B.; Knowles, T. P.; Biverstål, H.; Lendel, C.; Ekholm-Petterson, F.; Dubnovitsky, A.; Lannfelt, L.; Dobson, C. M.; Härd, T. *Proc. Natl. Acad. Sci. U. S. A.* **2010**, *107*, 15595−15600.
(38) Lendel.; et al. *Angew. Chem., Int. Ed.* **2014**, *53*, 12756−12760.
(39) Spencer, R. K.; Li, H.; Nowick, J. S. *J. Am. Chem. Soc.* **2014**, *136*, 5595−5598.
(40) Nowick, J. S.; Lam, K. S.; Khasanova, T. V.; Kemnitzer, W. E.; Maitra, S.; Mee, H. T.; Liu, R. *J. Am. Chem. Soc.* **2002**, *124*, 4972−4973.
(41) We also created a peptide with an *N*-methyl group at position F_{20}. This peptide forms oligomers with structures similar to those formed by peptide **1**.
(42) Spencer, R. K.; Nowick, J. S. *Isr. J. Chem.* **2015**, *55*, 698−710.
(43) Santiveri, C. M.; León, E.; Rico, M.; Jiménez, M. A. *Chem. - Eur. J.* **2008**, *14*, 488−499.
(44) Spencer, R. K.; Kreutzer, A. G.; Salveson, P. J.; Li, H.; Nowick, J. S. *J. Am. Chem. Soc.* **2015**, *137*, 6304−6311.
(45) Spencer, R.; Chen, K. H.; Manuel, G.; Nowick, J. S. *Eur. J. Org. Chem.* **2013**, *2013*, 3523−3528.
(46) Kabsch, W. *Acta Crystallogr., Sect. D: Biol. Crystallogr.* **2010**, *66*, 125−132.
(47) Weik, M.; Ravelli, R. B.; Kryger, G.; McSweeney, S.; Raves, M. L.; Harel, M.; Gros, P.; Silman, I.; Kroon, J.; Sussman, J. L. *Proc. Natl. Acad. Sci. U. S. A.* **2000**, *97*, 623−628.
(48) Leiros, H. K.; McSweeney, S. M.; Smalås, A. O. *Acta Crystallogr., Sect. D: Biol. Crystallogr.* **2001**, *57*, 488−497.
(49) The $^{\delta}$Orn in peptide **2** replaces K_{16} in Aβ. In a dodecamer of full-length Aβ, the side chain of K_{16} could form a salt bridge with the side chain of D_{23}.
(50) Pieters, B. J.; van Eldijk, M. B.; Nolte, R. J.; Mecinović, J. *Chem. Soc. Rev.* **2016**, *45*, 24−39.
(51) Butterfield, S. M.; Lashuel, H. A. *Angew. Chem., Int. Ed.* **2010**, *49*, 5628−5654.
(52) Glabe, C. G. *J. Biol. Chem.* **2008**, *283*, 29639−29643.
(53) Larson, M. E.; Lesné, S. E. *J. Neurochem.* **2012**, *120*, 125−139.
(54) Liu, P.; Reed, M. N.; Kotilinek, L. A.; Grant, M. K.; Forster, C. L.; Qiang, W.; Shapiro, S. L.; Reichl, J. H.; Chiang, A. C.; Jankowsky, J. L.; Wilmot, C. M.; Cleary, J. P.; Zahs, K. R.; Ashe, K. H. *Cell Rep.* **2015**, *11*, 1760−1771.
(55) Kayed, R.; Head, E.; Thompson, J. L.; McIntire, T. M.; Milton, S. C.; Cotman, C. W.; Glabe, C. G. *Science* **2003**, *300*, 486−489.
(56) Tao, Y.; Strelkov, S. V.; Mesyanzhinov, V. V.; Rossmann, M. G. *Structure* **1997**, *5*, 789−798.

DOI: 10.1021/jacs.6b01332
J. Am. Chem. Soc. 2016, 138, 4634−4642